Remote Sensing Applications: Society and Environment 28 (2022) 100850

Contents lists available at ScienceDirect

Remote Sensing Applications: Society and Environment

journal homepage: www.elsevier.com/locate/rsase

A simplified structure-from-motion photogrammetry approach for urban development analysis

Chima Iheaturu [a, *], Chukwuma Okolie [b], Emmanuel Ayodele [b], Andy Egogo-Stanley [b], Solomon Musa [c], Chinwe Ifejika Speranza [a]

[a] University of Bern, Institute of Geography, Bern, Switzerland
[b] University of Lagos, Department of Surveying and Geoinformatics, Lagos, Nigeria
[c] Federal Capital Development Authority, Department of Survey and Mapping, Abuja, Nigeria

ARTICLE INFO

Keywords:
Change detection analysis
Digital map creation
Geospatial methods
Parsimonious land use
Unmanned aerial vehicle (UAV)

ABSTRACT

Despite the increasing availability of remote sensing imagery, spatial data of adequate spatio-temporal resolution for urban development analysis and urban planning remains inadequate in some places. Structure-from-Motion (SfM) photogrammetry provides a low-cost option to generate such data at the desired spatial resolution. This study thus presents a simplified approach for mapping and performing urban development analysis in a suburban area (Kuje) in Abuja, Federal Capital Territory, Nigeria. Here, we compared a Google Earth® historical imagery of 2005 (baseline data) with SfM-derived imagery of 2019 (recent data) to quantify the rate and magnitude of urban development in the area. The Ground Control Points (GCPs) survey achieved a Root Mean Square Error (RMSE) of 31.01 mm and 24.34 mm in planimetry and elevation respectively while the SFM survey achieved an RMSE of 21.11 mm, 25.35 mm and 96.06 mm in the X, Y & Z coordinate axes respectively, which are within the acceptable limit (< 10 cm). The urban development analysis revealed that over the past 14 years, an average of 8 buildings were constructed per year. The area also witnessed an increase in the construction of roads and an associated decline in the green areas. In addition, the building height assessment revealed that land is not being used parsimoniously. The findings in this study demonstrate the viability of SfM photogrammetry in creating digital maps for small suburban areas and in performing urban development analysis. Furthermore, the results obtained can aid town planners and development authorities to make informed decisions about urban development issues in the area.

1. Introduction

Three-dimensional (3D) data acquisition in urban or suburban areas requires planning based on classical standards as well as the application of different surveying techniques that can complement each other (Koska and Křemen, 2013; Martínez-Espejo Zaragoza et al., 2017). The past two decades have witnessed extensive use of both airborne and terrestrial laser scanning (TLS) techniques to obtain very high resolution and high-quality 3D topographic data (Heritage and Hetherington, 2007; Hodge et al., 2009; Lohani and Mason, 2001). However, laser scanning requires expensive equipment and specialised skills to operate. In contrast, Structure-from-Motion (SfM) photogrammetry provides opportunities for a low-cost 3D model generation with little expertise (Caroti et al., 2015; Micheletti et al., 2015; Westoby et al., 2012). SfM photogrammetry is a low-cost approach for constructing 3D, geolocated terrain and object models from a set of multiple overlapping photographs acquired from moving cameras with or without ground reference points

* Corresponding author. University of Bern, Institute of Geography, Hallerstrasse 12, CH-Bern, 3012, Switzerland.
E-mail address: chima.iheaturu@giub.unibe.ch (C. Iheaturu).

https://doi.org/10.1016/j.rsase.2022.100850
Received 29 March 2022; Received in revised form 24 August 2022; Accepted 10 October 2022
Available online 13 October 2022

(Ostwald and Hurtado, 2017; Westoby et al., 2012). This is achieved by matching the textures in the images and determining the 3D geometry with the idea that the scene is static. The SfM process commences by acquiring photographs that converge on the object of interest with adequate overlap (for example, 60–80% overlap) between successive images as each point must be visible on a minimum of 3 images (Lucieer et al., 2014; Shervais, 2016; Westoby et al., 2012). This involves taking photographs from several positions and/or angles. Different types of imaging sensors can serve this purpose, from video stills to low-grade digital cameras (Smith and Vericat, 2015; Westoby et al., 2012) and smartphone cameras (Micheletti et al., 2015; Wrózyński et al., 2017).

SfM photogrammetry is now regarded as a valid alternative to traditional photogrammetry, Airborne Laser Scanning (ALS) and Terrestrial Laser Scanning (TLS) (Raoult et al., 2017). Its ability to extract accurate and high-resolution spatial data using low-cost cameras is remarkable (Fonstad et al., 2013; Micheletti et al., 2015; Tarolli, 2014). The emergence of SfM methods and their incorporation into classic stereoscopic photogrammetric surveys have transformed the creation of 3D terrain models. These models, when created are not only aesthetically fascinating but can also contain spatial information, whose quality is dependent on both the adopted survey technique and the processing steps used (Caroti et al., 2015; Smith et al., 2016). SfM deliverables include orthophotos, digital surface models (DSMs) and 3D point clouds. According to Rabiu & Waziri (2014), an orthophoto is a photograph that has been corrected for distortions in the camera lens, tilting of the camera during the photographic survey and relief distortions. In an orthophoto, true angles, areas and distances can be measured directly. Orthophotos provide accurate base maps which are important layers in a Geographic Information System (GIS). Orthophotos that have been scaled and georeferenced for accuracy are considered to be reliable for conducting precise measurements and calculations of objects of interest at a site. Also, due to the higher resolution and detail compared to typical satellite imagery, orthophotos are very useful for analysing the features of a large plot or area of land. With orthophotos and DSMs, one can create maps and models of construction projects, properties, and earthworks. Orthophotos are also very useful in feature extraction for map production or updating (Koeva et al., 2016), and change detection investigations (Gbopa et al., 2021; Sarp et al., 2014), city monitoring and disaster management as well as generating 3D models (Qin, 2014). In comparison with satellite images, Unmanned Aerial Vehicle (UAV) data offers advantages in terms of spatio-temporal resolution and cloudlessness (Qin, 2014; Yao et al., 2019). UAV images provide precise data measurements (Franklin and Wulder, 2002; Jumaat et al., 2018), that enable the accurate processing of variations in urban land cover.

To date, vast urban and suburban areas of Nigeria are relatively unmapped. Although, standard topographic maps are routinely produced by the Office of the Surveyor-General of the Federation (OSGOF) at scales of 1:25,000, 1:50,000 and 1:100,000; these maps are unable to capture changes and developments occurring in small spatial units. In particular, the maps are unable to show if the land is being used parsimoniously to cater for the growing population in the urban and suburban areas as the developments are usually classified as built-up areas. Therefore, it is imperative to take advantage of modern technologies such as UAVs, which enable the fast creation and update of digital maps for rapid decision making. In this context, this study presents a simplified approach for mapping and performing urban development analysis in a suburban area (Kuje) in Abuja, Nigeria, by utilising SfM photogrammetry with Google Earth® historical imagery; illustrating the steps required to generate an Orthomosaic (combination of several orthophotos) and DSM, starting from the initial acquisition of photos using a low-cost UAV to the analysis and utilisation stage. The goal is to outline a practical workflow that could be adopted by geospatial information scientists, urban planners and development authorities to quantify urban development. In addition, the paper assesses the heights of buildings to ascertain if the land is being used parsimoniously. To achieve this, this paper presents a workflow (Fig. 1) that uses DroneDeploy® (a mobile-based application that runs on both Android and IOS) for flight planning, a low-cost UAV (DJI Mavic 2 Pro) for photographs acquisition, and PIX4Dmapper® desktop software (version 4.4.12) for photographs processing to produce orthophoto and DSM. The choice of the UAV for acquiring the recent imagery is justified by its ability to generate both an Orthomosaic and a DSM from which building heights can be measured. Although Google Earth® has a "3D buildings" layer, this feature is however not available for the study area.

2. Materials and methods

2.1. Study area

The study area shown in Fig. 2 is located within Kuje Area Council in Abuja, the Federal Capital Territory (FCT), Nigeria. Kuje is about 40 km southwest of Abuja municipality and lies between longitudes 8° 52′ 37″ E to 8° 52′ 54″ E and latitudes 7° 14′ 7″ N to 7° 14' 28" N. Kuje has an area of approximately 1644 km^2 and a population of 97,367 based on the last census conducted in 2006. It is one of the rapidly developing suburbs in Abuja mainly because of its proximity to Abuja Municipal Area Council (AMAC) and the Nnamdi Azikwe International Airport, Abuja, as well as the Kuje prison. In Kuje, the cost of accommodation is low compared to other suburbs close to the municipality, and foodstuffs are also cheaper due to its surrounding agrarian communities.

Abuja is a planned city and was built mainly in the 1980s, replacing the country's most populous city of Lagos as the capital on December 12, 1991. The main reason for the relocation was to develop a new capital city that is free from social and environmental challenges associated with the former capital, Lagos (Enoguanbhor et al., 2022). However, Abuja grew by 139.7% between 2000 and 2010, making it at that time, the fastest-growing city in the world (Boumphrey, 2010). The population of Abuja has continued to grow at a rate (5.67% per annum) that exceeds the national population growth rate (2.5% per annum) and it is projected to reach 11 million by 2035 (World Bank, 2021). Following this trend, and to accommodate the growing population of Abuja, it is noted that suburbs such as Kuje will experience an exponential increase in urban development in the coming years.

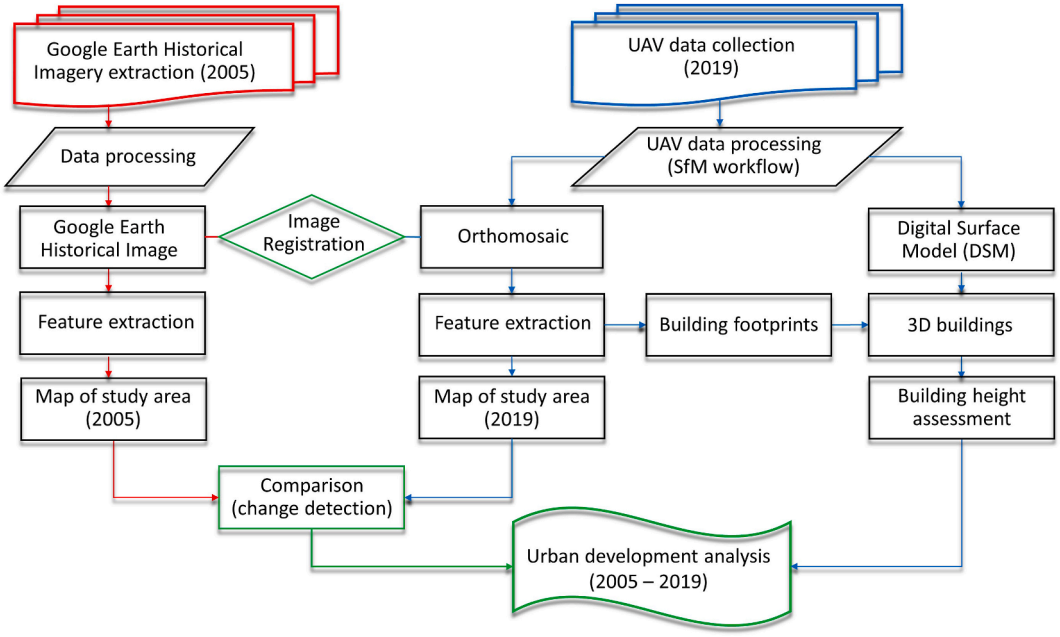

Fig. 1. Methodology flowchart of the main steps for the urban development analysis.

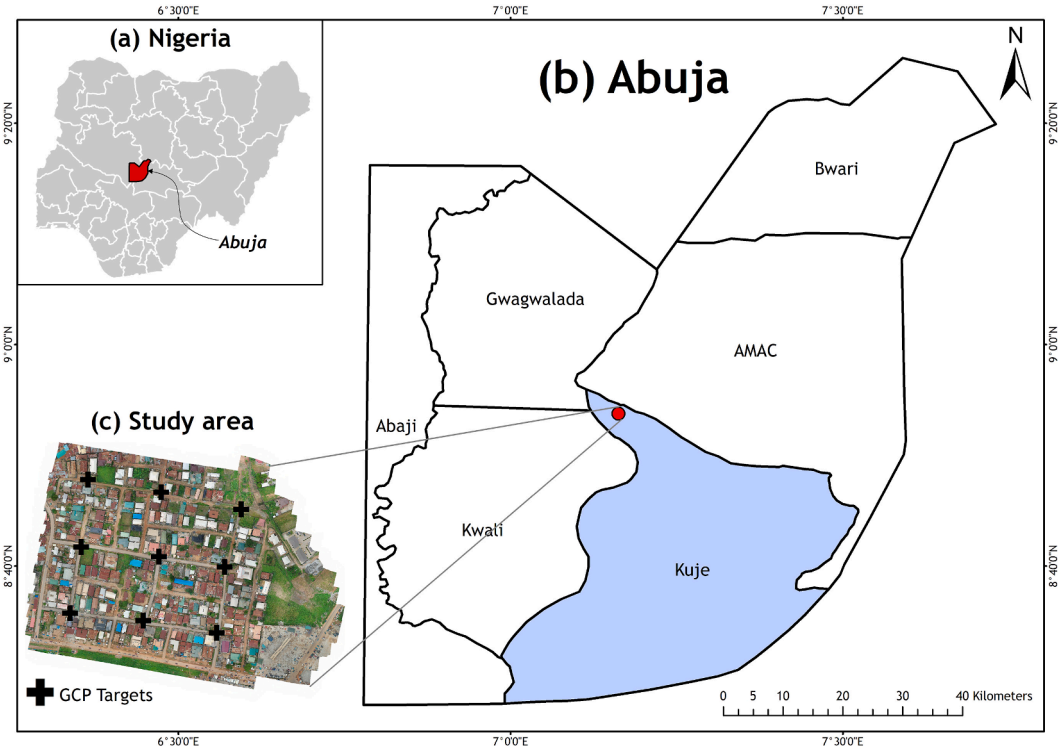

Fig. 2. (a) Map of Nigeria showing the location of Abuja (highlighted in red), (b) Map of Abuja showing the location of Kuje (highlighted in blue) and the location of the study area (indicated with a red dot), and (c) Orthomosaic of the study area showing the spatial distribution of the GCPs targets. (For interpretation of the references to colour in this figure legend, the reader is referred to the Web version of this article.)

2.2. Data collection

2.2.1. UAV imagery

A low-cost UAV (DJI Mavic 2 Pro) was used to capture the images of a small section of Kuje (Fig. 1). The DJI Mavic 2 Pro features omnidirectional vision systems and infrared sensing systems; and it captures complex shots using signature DJI technologies (DJI,

2019). The UAV camera lens has a focal length of 35 mm and a sensor of 20 megapixels (1" CMOS). The DJI Mavic 2 Pro is equipped with an in-built Global Navigation Satellite System (GPS and GLONASS) with a hovering accuracy range; vertical: ± 0.1 m (when vision positioning is active), ±0.5 m (with GPS positioning) and horizontal: ± 0.3 m (when vision positioning is active) and ±1.5 m (with GPS positioning). The in-built GNSS allows the UAV to capture geolocated images, which helps to reduce processing time (PIX4D, 2017).

To produce a model with good accuracy, the UAV survey must have multiple viewpoints, adequate overlap (60% front overlap and 75% side overlap), and a sufficient number of GCPs well distributed in the area of interest (Iheaturu et al., 2020). Hence, nine targets were evenly distributed across the study area (see Fig. 2). These targets were fabricated using white PVC (polyvinyl chloride) material coated with a matte finish to prevent glare. The GCP coordinates were then measured using a Hi-target V30 GNSS (Global Navigation Satellite System) unit in Real-Time Kinematic (RTK) mode. Fig. 3 shows one of the GCP targets used in the study.

The flight path was predefined on the DroneDeploy® software installed on a mobile device that was attached to the remote controller of the UAV. The flight path was designed in such a way that it slightly extends beyond the boundary of the study site to ensure full coverage. The UAV home point was set approximately at the start of the flight path and a flying height of 61 m was set. This height was chosen because of potential interference with two telecom masts (55 m tall) seen at the site. Also, this height allowed the UAV to acquire fewer images, which is expected to reduce the image processing time (Torres-Sánchez et al., 2018). The UAV flew for 25 min 41 s capturing a total of 470 images covering an area of 22.55 ha (0.23 km^2). The degree of overlap for the survey was maintained at 60% (forward) and 75% (side). Fig. 4 shows some of the individual images captured during the flight.

2.2.2. Google Earth historical imagery

By default, Google Earth® displays the most recent images available in its database. However, with the historical imagery tool, one can also see what the scene looked like in the past; though this option may not be available for every location. Archive images are mainly used to detect changes over time for a particular region. These images could be downloaded in parts using specialised software such as the open-source software called Elshayal Smart GIS (Elshayal, 2021). The Elshayal Smart GIS Software was linked to Google Earth® and thus used in extracting the 2005 Google Earth historical image.

The choice of 2005 Google Earth® imagery was borne out of the unavailability and inaccessibility of other map sources for the period under consideration as well as the need to carry out urban development analysis in the study area for at least 14 years to understand changes over time. Changes within that period will give insights into the rate and/or type of development and thus, inform policy formulation as well as facilitate informed decisions on urban planning.

2.3. UAV data processing and quality assessment

The 3D coordinates acquired from the GPS survey, and the images acquired from the UAV survey were downloaded, uncompressed and saved. The images were imported into the PIX4Dmapper® software and used to generate the initial sparse 3D point cloud. PIX4Dmapper® runs on a 64-bit Microsoft Windows operating system, and the RAM requirement varies with the size and number of photographs as well as the density of the reconstruction. However, the 3D reconstruction described in this paper was done on a Windows 10 Laptop with the following specifications - Intel(R) Pentium(R) CPU N3710 @ 1.60 GHz, 8 GB-RAM and 2 TB hard disk drive.

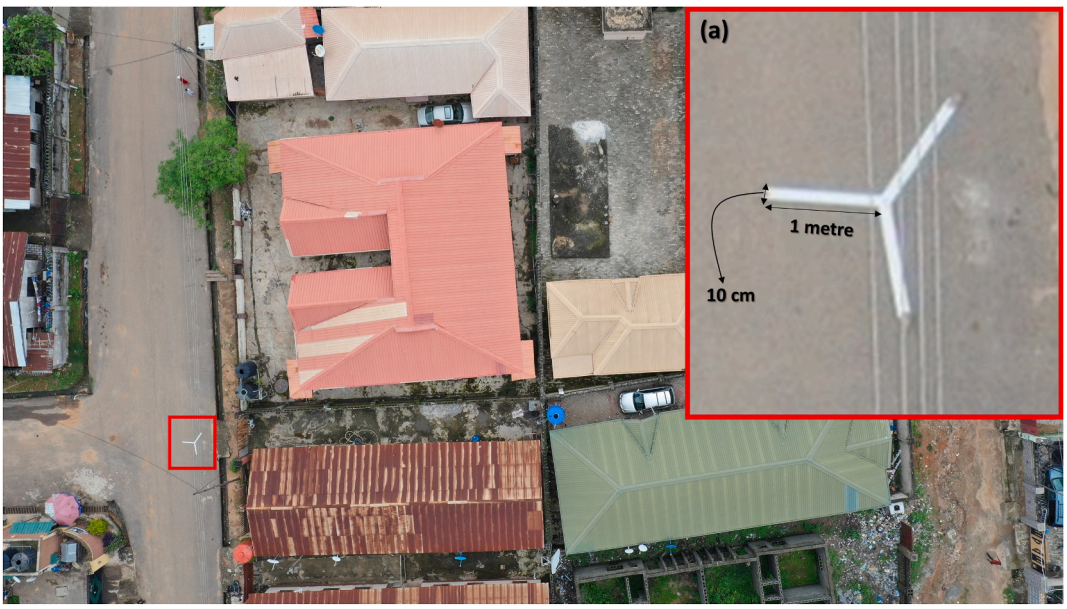

Fig. 3. A GCP target (within the red box) in the study area, (a) Magnified view of the GCP target showing the dimensions. (For interpretation of the references to colour in this figure legend, the reader is referred to the Web version of this article.)

Fig. 4. A view of some of the UAV-acquired images showing feature overlap between adjacent images. The same features are numbered identically.

The SfM workflow within PIX4Dmapper® starts with the initial processing, which handles the image alignment. The main aim of this process is to produce a sparse 3D point cloud. In this stage, the program (through the built-in SiftGPU algorithm) identifies and matches feature key points, which are automatically tracked through the entire photo set (Lowe, 2004). The geometry of the scene is reconstructed with these matched key points. All the matched points make up the sparse point cloud (See Fig. 5). The target positions in Comma Separated Value (*.csv) format was imported into ArcMap® and overlaid on a base map to view their spatial distribution. The target coordinates were imported and matched on the images (georeferenced) using the rayCloud Editor tool in the PIX4Dmapper®. Targets were verified through inspection of the base map in the ArcMap® environment. The point cloud data were then re-matched and optimised. Thereafter, a quality report was generated. The generated quality report revealed that the georeferencing was within the allowable limit (<0.1 m) in line with Smith et al. (2016). After the target marking was complete, the type was then

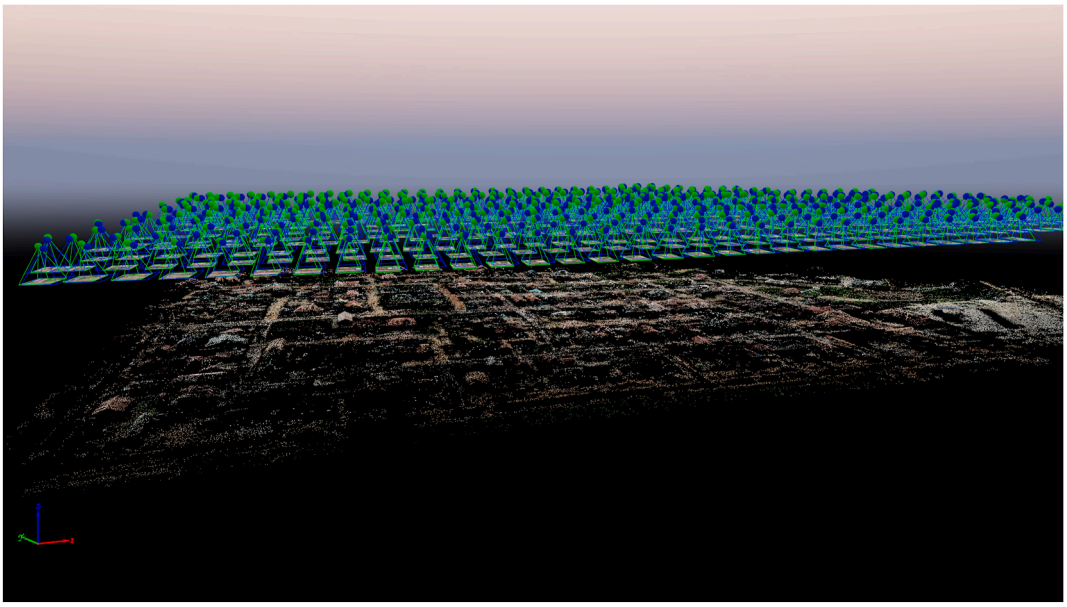

Fig. 5. Sparse point cloud generated in the initial processing stage (Screenshot from PIX4Dmapper® software).

changed to "Check Point" and then re-matched and optimised following a methodology described in PIX4D (2017). The next step was the point cloud generation. To reduce the processing time, the images were resampled to a quarter of their original resolution, and the densified point clouds generated were saved in the LiDAR file format (*.las). This resampling was done in line with the principle of economy of accuracy, given that such a resolution is accurate enough for further analysis. Finally, an Orthomosaic and a DSM were generated and saved in GeoTiff file format (*.tif).

To assess the quality of the SFM-derived model, it is often compared against those derived from established techniques of higher accuracy such as Total Station, GPS survey, TLS etc. (James and Quinton, 2014; Smith et al., 2016; Smith and Vericat, 2015). Thus, we validated the point cloud data using the 3D coordinates of the targets measured using RTK GPS. All the nine GCPs were used as "checkpoints" to assess the absolute accuracy of the point cloud. The following metrics were computed to describe the accuracy: Mean, Standard Deviation – S. D (σ), and Root Mean Square Error (RMSE).

2.4. Image registration

The UAV images acquired were referenced to the Minna datum, the origin of the Nigerian coordinates system and projected using the UTM projection system. However, the Google Earth® 2005 satellite image was acquired in the WGS84 coordinate system. Such disparities hamper easy comparison between the images, thus emphasising the need for harmonisation in the coordinate systems. This was first addressed using transformation techniques in ArcGIS® software i.e., transforming the coordinate system of the GE Historical Imagery from WGS84 to UTM Zone 32 (Minna). However, there were some slight tilts and shifts due to the transformation. Hence, the GE Historical Imagery was shifted (via image registration) to align with the Orthomosaic before the vectorisation process.

Remote sensing analysis such as change detection requires image-to-image registration to facilitate comparison (Ezzeldeen et al., 2010). This process allows two or more images that were possibly taken at different periods, using different sensors, to have their spatial correspondence established to match them (Lubansky, 2011). In this study, both images (the 2005 and the 2019 images) were aligned geometrically to enhance comparison. The procedure was carried out using manually selected coincident points on both images, with the aid of identifiable features/monuments.

2.5. Feature extraction

The high spatial resolution of the imageries (GE Historical Image and Orthomosaic) made it possible for features of interest to be easily identified and delineated. In this study, features such as building footprints, roads and plots (extrapolated from fences) were regarded as indicators of urban development and were thus digitised into shapefile layers created in ArcMap® software. Here the imageries were displayed as the screen backdrop and then the geometries of the features were defined by digitising from the screen using a cursor controlled by the mouse. The building footprints were classified as either completed or uncompleted, the roads were classified as either tarred or untarred and the plots were classified as either developed or undeveloped to help understand the urban development. This method of manual digitisation was preferred to the automatic and semi-automatic image classification methods (e.g., object-oriented image classification) because of the relatively small study area (22.55 ha) and the level of precision achievable.

2.6. Urban development analysis

The urban development analysis performed in this study focused on assessing the urban developments (in terms of physical structures) that have occurred within the period (2005–2019). We compared the features in 2005 with those in 2019 to determine the magnitude and rate of urban development. The count of the completed buildings, as well as the buildings under construction as of 2005, was compared with a more recent (2019) count to quantify the changes. Similarly, we compared the plots (developed and undeveloped) as well as the roads (tarred and untarred) in 2005 with those in 2019. The building count ratio and plot-status ratio helped to obtain a clear picture of the urban development trend over the years. Also, the length of the tarred and untarred roads served as a measure of ascertaining the rate and magnitude of change in the study area over time (2005–2019).

Furthermore, we evaluated the percentage distribution of the building heights to ascertain if the land is used parsimoniously. We expect that taller buildings will house more people on an acre of land and consequently improve land preservation (Ali and Al-Kodmany, 2012). Conversely, an area that is predominantly occupied by bungalows (small buildings) will house fewer people and ultimately increase the demand for more housing units. Thus, to ascertain if the land is used parsimoniously, we extracted the heights of the buildings from the 2019 SFM-derived DSM and calculated their distribution ratio.

3. Results and discussion

3.1. UAV data processing and quality assessment results

3.1.1. Ground control points

Table 1 presents both the planimetric and elevation errors in the GCP coordinates. The GCP coordinates acquired using RTK GNSS are expected to have positional error between $\pm$20–80 mm in line with the Royal Institution of Chartered Surveyors, (2010). However, the positional errors obtained range from 18.73 mm at GCP004 to 49.84 mm at GCP006. The results show that all the errors were within the acceptable limit ($<$80 mm). Hence, the dataset was deemed fit for purpose considering the extent and nature of the study area.

3.1.2. Image calibration

All the 470 images were calibrated, which translates to a 100% calibration. Similarly, all the images were geolocated and enabled. Pix4D® extracts EXIF (Exchangeable Image File Format) data from each image to gain information about the camera parameters

Table 1
Errors in the GCP coordinates.

GCPs	Position error (mm)	Elevation error (mm)
GCP001	20.92	32.85
GCP002	47.38	−19.78
GCP003	27.47	−12.88
GCP004	18.73	−27.37
GCP005	18.94	32.22
GCP006	49.84	36.76
GCP007	30.44	−15.01
GCP008	24.22	−10.36
GCP009	22.54	−15.00
RMSE (mm)	**31.01**	**24.34**

(e.g., skew, focal length, image size, principal point and often radial distortion parameters), which is used to determine the camera's position (Morgan and Brogan, 2016; Smith et al., 2016). As seen in Fig. 6, which was extracted from Pix4D® software, images were captured regularly along the predefined flight path.

The number of keypoint matches in a photograph is based on the texture and resolution of the image, such that complex images at high resolutions will get the best results (Westoby et al., 2012). Fig. 7 (a) shows the computed image positions with links between matched images. Bright links indicate fewer keypoint matches between the images while the darker links indicate more keypoint matches between the images. The number of keypoint matches influences the quality of the Orthomosaic i.e., areas with fewer keypoint matches are likely to have poor quality results (Liu et al., 2018). This can be seen in Fig. 7 (b) which was extracted from the quality report generated by the PIX4Dmapper® software. In Fig. 7 (b), areas with fewer overlapping images (i.e., the yellow, orange and red areas) coincided with areas with weak links in Fig. 7 (a), while the areas coloured in green (indicating an overlap of 4–5 + images per pixel) coincided with the areas with more keypoint matches in Fig. 7 (a). However, the delineated area of study was mainly covered in green (except the fringes), indicating that the results obtained are generally good according to Lim et al. (2021).

3.1.3. Orthomosaic and DSM

Figs. 8 and 9 show the generated Orthomosaic and DSM respectively. As expected, the Orthomosaic and DSM were generated at a Ground Sampling Distance (GSD) of 1.43 cm (0.56 in). That is, one pixel in the image represents (linearly) 1.43 cm on the ground, meaning that an object as small as 1.43 cm can be identified on the image. This is evident in the visible features in the Orthomosaic (See Fig. 8 (a)). The GSD is influenced by the flight height and the specification (i.e., Image width, sensor width, and focal length) of the UAV camera sensor. This value is often predetermined by the flight planning software before the UAV flight i.e., once the flying height is set, the system automatically calculates the expected GSD using the UAV camera specifications. The low GSD also influenced the resolution and output quality of the DSM generated (Fig. 9). With the high level of detail (LOD), the geometry of the rooftop can be easily visualised (Fig. 9 (a)).

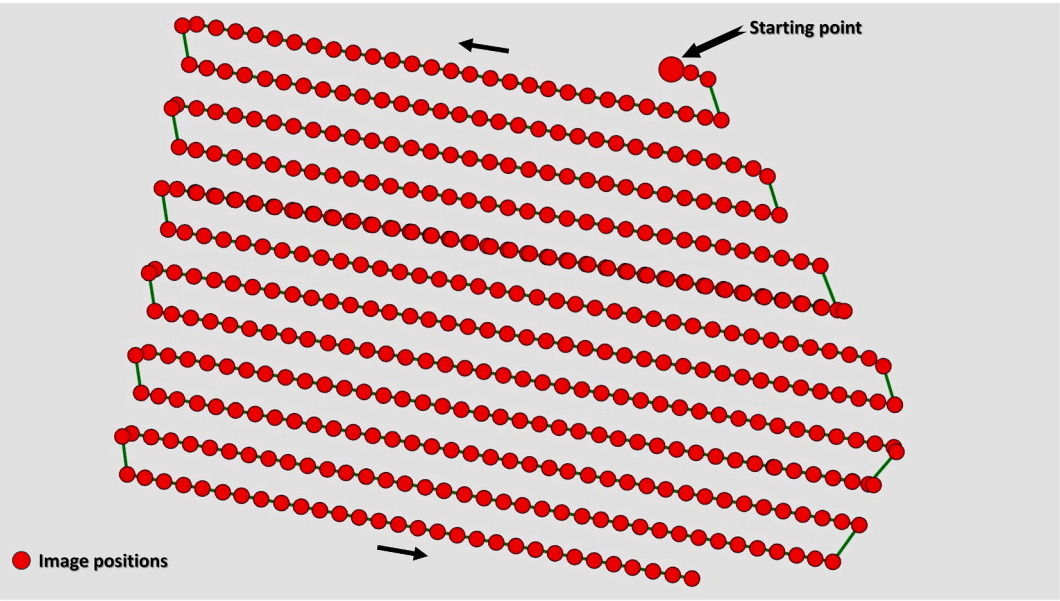

Fig. 6. Top view of the initial image position. The green line follows the position of the images in time starting from the large red dot. (For interpretation of the references to colour in this figure legend, the reader is referred to the Web version of this article.)

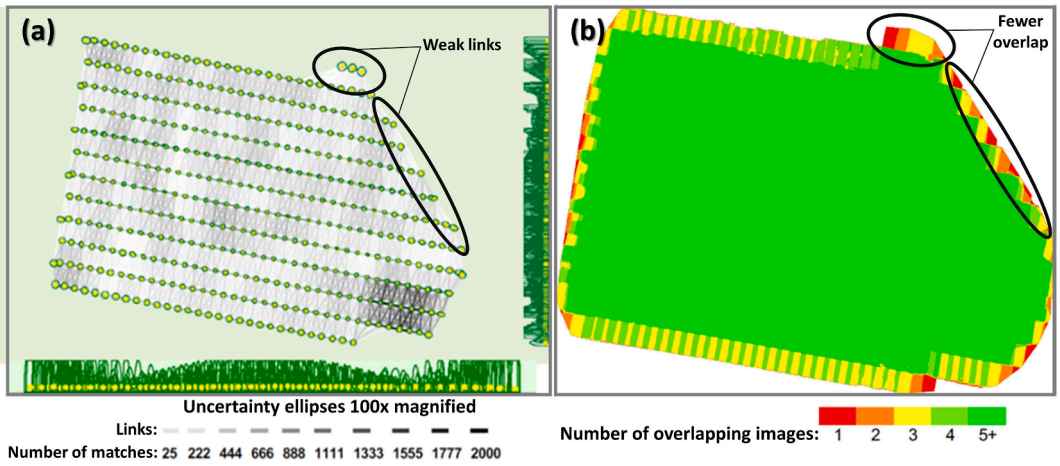

Fig. 7. (a) Computed image positions with links between matched images (some weak links are indicated using the black ellipses), (b) Number of overlapping images computed for each pixel of the Orthomosaic (areas with fewer overlap are indicated using black ellipses).

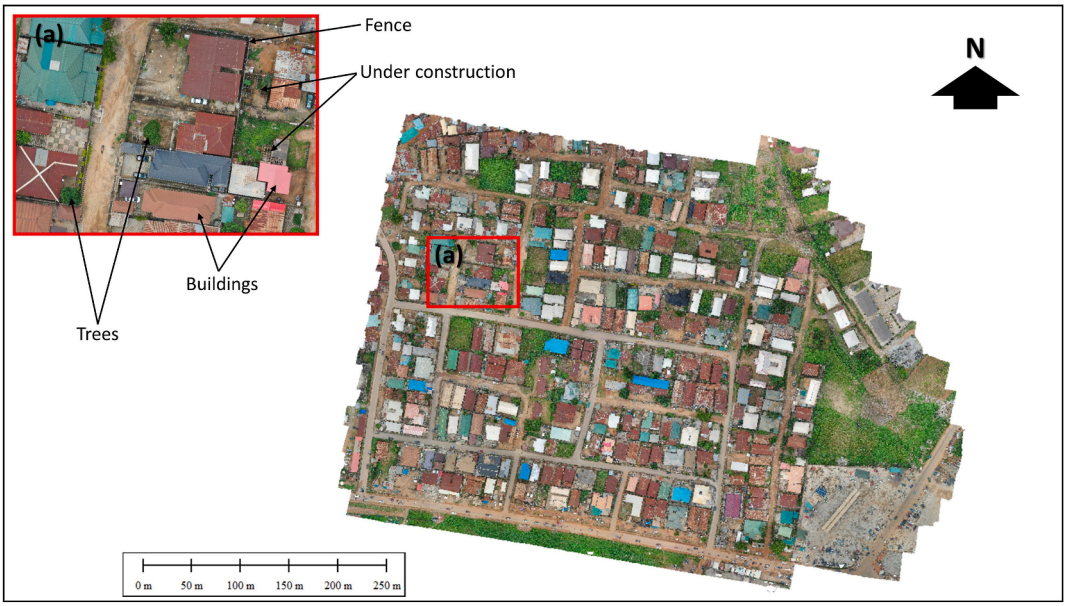

Fig. 8. Orthomosaic of the study area (2019), (a) Magnified view of a section showing different visible features.

Flying at a low altitude improves the GSD of the Orthomosaic and DSM (Abou Chakra et al., 2020; Doumit, 2018; Leitão et al., 2016). However, this will also increase the number of images captured, the number of batteries used as well as the processing time (Abou Chakra et al., 2020). The low flying height (61 m) chosen for this study was optimal for the relatively small area. However, for larger projects that do not need a high LOD, it is recommended to fly higher to minimise the number of images acquired (Ali and Abed, 2019).

3.1.4. Accuracy assessment

Georeferencing the SfM survey accurately is an essential aspect of SfM validation to ensure its reliability for various geoscience applications (Caroti et al., 2015). The SfM-based survey employed nine GCPs which were measured using RTK GPS. These GCPs were used to georeference the point clouds generated. As earlier mentioned, the validation dataset was based on the RTK GPS-derived coordinates of the target crosshairs. The RMSEs in the horizontal and vertical positions of the targets (GCPs) were derived as 31.01 mm and 24.34 mm respectively (see Table 1). Table 2 presents the point-to-point validation details using all the nine (9) GCPs as checkpoints as this improves the accuracy (Iheaturu et al., 2020). The accuracy of UAV surveys is expected to be in the range of 5–10 cm in the horizontal (X, Y) position and 5–15 cm in the vertical (Z) position (Elkhrachy, 2021; Vautherin et al., 2016). However, the accuracy values obtained for the mean, standard deviation and RMSE were all less than 10 cm, which is an indication that the results are reliable and useable.

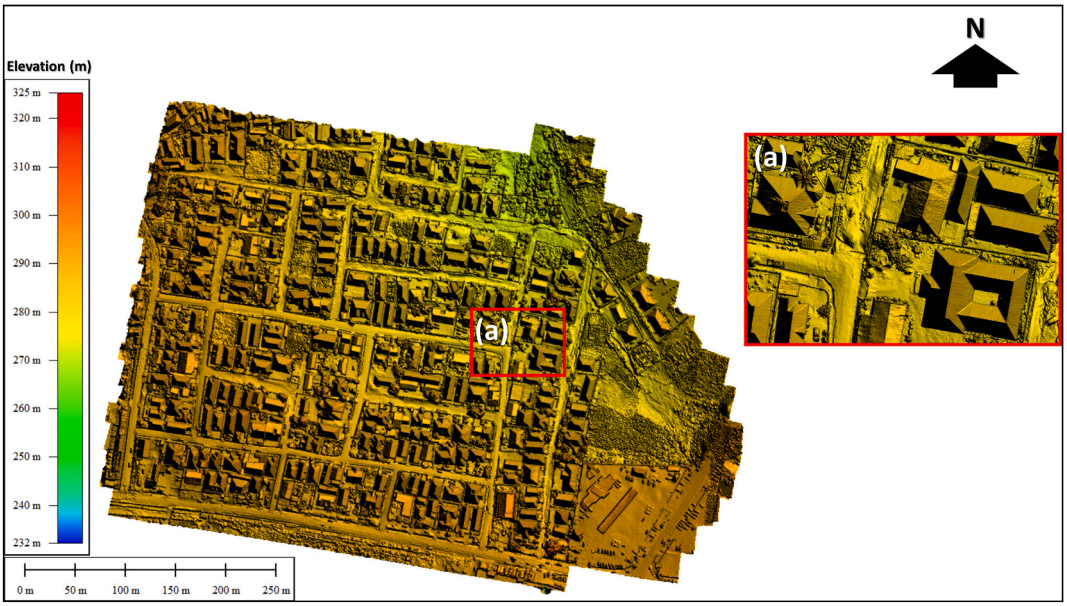

Fig. 9. Digital Surface Model (DSM) of the study area (2019), (a) Magnified view showing the detailed 3D reconstruction.

Table 2
Point to Point validation results (using 9 checkpoints).

Accuracy indices	Error X (mm)	Error Y (mm)	Error Z (mm)
Mean	5.62	14.31	−91.85
SD	20.35	20.92	28.13
RMSE	21.11	25.35	96.06

3.2. Urban development 2005–2019

The extracted road features were populated with attributes such as road names, which were recorded during a site visit. Digital maps were then produced in ArcMap®, one for 2005 (Fig. 10a) and another for 2019 (Fig. 10b). From the maps, we can observe that some urban developments occurred during the period of study. For example, several plots, which were undeveloped in 2005 were developed in 2019. The magnitude of the changes that occurred within the period of study (2005–2019), as well as the rate of the said changes, can be seen in Table 3. The percentage distribution of buildings (Table 3) across the study area within the period of the study showed that in the year 2005, there were 200 buildings, 185 (92.5%) fully erected and 15 (7.5%) under construction. The number of buildings increased to 320 in the year 2019, with 313 (97.81%) fully completed and 7 (2.19%) under construction. Between 2005 and

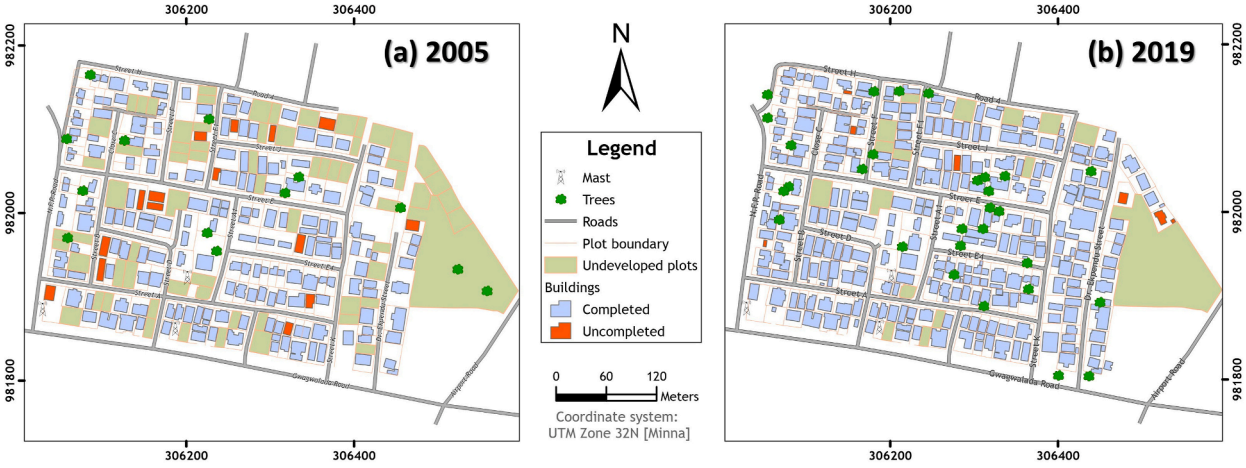

Fig. 10. (a) 2005 digitised map from the extracted Google Earth® Historical Image, and (b) 2019 digitised map from the Orthomosaic.

Table 3
Comparison between the digital map of 2005 and that of 2019.

Category	Year - 2005	Year - 2019	Change	Rate
Completed buildings	185.00	313.00	128.00	8 new buildings per year
Uncompleted buildings	15.00	7.00	−8.00	
Total number of buildings	200.00	320.00	120.00	
Developed plots	182.00	234.00	52.00	3 plots developed per year
Undeveloped plots	68.00	16.00	−52.00	
Total number of plots	250.00	250.00	0.00	
Tarred road length (m)	1199.25	2781.77	1582.52	7 m road per year
Roads not tarred (m)	3334.72	1864.62	−1470.09	
Total road length (m)	4533.97	4646.39	112.42	
Undeveloped area (m^2)	35992.33	17334.65	−18657.68	1243.8m^2 developed per year
Developed area (m^2)	120198.08	138855.76	18657.68	
Area of study (m^2)	156190.41	156190.41	0.00	

2019, the number of buildings increased by 120. All the buildings that were previously under construction in 2005 are now fully completed in 2019.

The study area was divided into 250 plots based on the visible demarcations (fences) on the Orthomosaic. In 2005, only 182 (72%) of the plots had been developed and by 2019, another 52 plots had been developed, leading to a total of 234 plots. The study area occupies a total area of 156190.41 m^2. In 2005, 23.04% of this area was undeveloped. However, the period of the study recorded a decrease in undeveloped land (11.10% in 2019).

The study area also witnessed some infrastructural development within the period (2005–2019) in terms of transportation as can be seen in the road networks with an additional length of 1.5 km of tarred road (See Table 3). The increase in the total length of roads is explained by the need to access the newly developed plots.

3.2.1. Three-dimensional (3D) building assessment

Fig. 11 presents the 3D view of the study site showing the heights of different structures in varied colours. The colours depict heights in the range of 4 m (purple), 8 m (red) and >8 m (blue). An attribute query revealed that 98 buildings out of 320 (30.6%) have heights less than 4 m above the ground while 219 (68.4%) are less than 8 m above the ground. Also, only 3 buildings (1%) have heights greater than 8 m. This indicates that most of the structures within the study site are of low height. The building height variation can aid in decision making such as the need for better utilisation of land as explained by Bruyns et al. (2021), where the need for volumetric optimisation of available space is emphasised. The planners of Abuja, in their quest for sustainable urban development, need to shift their focus to vertical urban development as against lateral development. This will reduce the risk of exhausting the limited urban land resources considering the fast-growing population and the fact that land is a scarce natural resource.

Fig. 11. 3D view of the buildings within the study area (2019).

4. Conclusion

A simplified procedure utilising SfM photogrammetry to produce an orthophoto, DSM, a large-scale digital map and urban development analysis has been presented. The workflow presented offers non-expert users the ability to effectively produce maps of sub-urban areas and perform urban development analysis of small study areas without incurring the high cost of data acquisition or extensive fieldwork; thus, increasing the extent and frequency of surveys and map revisions. The Orthomosaic with an RMSE of 21.11 mm and 25.35 mm in the horizontal and vertical positions is adequate for digital mapping. The achieved topographic detail and quality are ideal for 3D mapping of sub-urban areas and townships. Furthermore, the study found that land is not being used parsimoniously in that only 1% of the buildings are above 8 m. Finally, the results of this study can contribute to knowledge-based decision-making for urban planning activities in the area.

The scope of this study was limited to the presentation of a simplified workflow that combined the use of SfM photogrammetry and Google Earth® historical images to conduct urban development analysis. Due to data scarcity, the study did not compare the 3D building model of 2005 with that of 2019. The study assumed that the buildings with the same roof shape and texture remained unchanged in the study period (2005–2019). Similarly, the study did not compare the observed urban developments with the master plan for the area. Thus, further research is needed to ascertain if the developments conform with the master plan. In addition, future studies should work on defining standards and best practices for the integration of UAV technology in urban planning and land administration workflows, and work on regulations to achieve parsimonious use of land.

Funding

This research did not receive any specific grant from funding agencies in the public, commercial, or not-for-profit sectors.

Ethical Statement

The authors declare that all ethical practices have been followed in relation to the development, writing, and publication of the article.

CRediT author statement

Chima Iheaturu: Conceptualisation, Formal analysis, Methodology, Visualisation, Writing - original draft, Writing – review & editing. **Chukwuma Okolie**: Conceptualisation, Formal analysis, Methodology, Visualisation, Writing - review & editing. **Emmanuel Ayodele**: Supervision, Writing - review & editing. **Andy Egogo-Stanley:** Methodology, Visualisation, Writing - Review and editing. **Solomon Musa:** Methodology, Writing - Review and editing. **Chinwe Ifejika Speranza:** Supervision, Writing - review & editing.

Declaration of competing interest

The authors declare that they have no known competing financial interests or personal relationships that could have appeared to influence the work reported in this paper.

Data availability

The data is made available in the accompanying Data in Brief article

Acknowledgements

The authors deeply appreciate the support received from the survey team of Pairs Geotechnics Nigeria Ltd. We also wish to thank Pix4Dmapper® for their free and accessible help files and all anonymous reviewers whose useful comments and suggestions were key to the success of this manuscript.

References

Abou Chakra, C., Somma, J., Gascoin, S., Fanise, P., Drapeau, L., 2020. Impact of flight altitude on unmanned aerial photogrammetric survey of the snow height on mount Lebanon. Int. Arch. Photogrammetr. Rem. Sens. Spatial Inf. Sci. ISPRS Arch. 43 (B2). https://doi.org/10.5194/isprs-archives-XLIII-B2-2020-119-2020.

Ali, H.H., Abed, F.M., 2019. The impact of UAV flight planning parameters on topographic mapping quality control. IOP Conf. Ser. Mater. Sci. Eng. 518 (2), 022018. https://doi.org/10.1088/1757-899X/518/2/022018.

Ali, M.M., Al-Kodmany, K., 2012. Tall buildings and Urban habitat of the 21st century: a global perspective. Buildings 2 (4). https://doi.org/10.3390/buildings2040384.

Boumphrey, S., 2010. World's Fastest Growing Cities Are in Asia and Africa - Euromonitor International Blog March 2. https://web.archive.org/web/20151117022953/http://blog.euromonitor.com/2010/03/special-report-worlds-fastest-growing-cities-are-in-asia-and-africa.html.

Bruyns, G.J.B., Higgins, C.D., Nel, D.H., 2021. Urban volumetrics: from vertical to volumetric urbanisation and its extensions to empirical morphological analysis. Urban Stud. 58 (5). https://doi.org/10.1177/0042098020936970.

Caroti, G., Martínez-Espejo Zaragoza, I., Piemonte, A., 2015. Accuracy assessment in structure from motion 3D reconstruction from UAV-born images: the influence of the data processing methods. Int. Arch. Photogrammetr. Rem. Sens. Spatial Inf. Sci. ISPRS Arch. 40 (1W4). https://doi.org/10.5194/isprsarchives-XL-1-W4-103-2015.

DJI, 2019. Mavic 2 PRO/ZOOM User Manual V2.0. https://dl.djicdn.com/downloads/Mavic_2/20190417/Mavic_2_Pro_Zoom_User_Manual_v2.0_en.pdf.

Doumit, J.A., 2018. Multiscale landforms classification based on UAV datasets. Sustain. Environ. 3 (2). https://doi.org/10.22158/se.v3n2p128.

Elkhrachy, I., 2021. Accuracy assessment of low-cost unmanned aerial vehicle (UAV) photogrammetry. Alex. Eng. J. 60 (6). https://doi.org/10.1016/j.aej.2021.04.011.

Elshayal, M., 2021. Elshayal Smart GIS Software (21.02. https://elshayal-smart.en.lo4d.com/windows.

Enoguanbhor, E.C., Gollnow, F., Walker, B.B., Nielsen, J.O., Lakes, T., 2022. Simulating urban land expansion in the context of land use planning in the Abuja city-

region, Nigeria. Geojournal 87 (3). https://doi.org/10.1007/s10708-020-10317-x.
Ezzeldeen, R.M., Ramadan, H.H., Nazmy, T.M., Yehia, M.A., Abdel-Wahab, M.S., 2010. Comparative study for image registration techniques of remote sensing images. Egypt. J. Rem. Sens. Space Sci. 13 (1). https://doi.org/10.1016/j.ejrs.2010.07.004.
Fonstad, M.A., Dietrich, J.T., Courville, B.C., Jensen, J.L., Carbonneau, P.E., 2013. Topographic structure from motion: a new development in photogrammetric measurement. Earth Surf. Process. Landforms 38 (Issue 4). https://doi.org/10.1002/esp.3366.
Franklin, S.E., Wulder, M.A., 2002. Remote sensing methods in medium spatial resolution satellite data land cover classification of large areas. Prog. Phys. Geogr. 26 (2). https://doi.org/10.1191/0309133302pp332ra.
Gbopa, A.O., Ayodele, E.G., Okolie, C.J., Ajayi, A.O., Iheaturu, C.J., 2021. Unmanned aerial vehicles for three-dimensional mapping and change detection analysis 6. Geomatics Environ. Eng. 15 (1). https://doi.org/10.7494/geom.2021.15.1.41.
Heritage, G.L., Hetherington, D., 2007. Towards a protocol for laser scanning in fluvial geomorphology. Earth Surf. Process. Landforms 32 (1). https://doi.org/10.1002/esp.1375.
Hodge, R., Brasington, J., Richards, K., 2009. In situ characterization of grain-scale fluvial morphology using Terrestrial Laser Scanning. Earth Surf. Process. Landforms 34 (7). https://doi.org/10.1002/esp.1780.
Iheaturu, C.J., Ayodele, E.G., Okolie, C.J., 2020. AN assessment of the accuracy of structure-from-motion (SFM) photogrammetry for 3D terrain mapping. Geomatics Landmanag. Landsc. 2, 65–82. https://doi.org/10.15576/gll/2020.2.65.
Royal Institution of Chartered Surveyors, 2010. Guidelines for the use of GNSS in land surveying and mapping. 06 6. https://www.rics.org/uk/upholding-professional-standards/sector-standards/land/guidelines-for-the-use-of-gnss-in-land-surveying-and-mapping/.
James, M.R., Quinton, J.N., 2014. Ultra-rapid topographic surveying for complex environments: the hand-held mobile laser scanner (HMLS). Earth Surf. Process. Landforms 39 (1). https://doi.org/10.1002/esp.3489.
Jumaat, N.F.H., Ahmad, B., Dutsenwai, H.S., 2018. Land cover change mapping using high resolution satellites and unmanned aerial vehicle. IOP Conf. Ser. Earth Environ. Sci. 169 (1). https://doi.org/10.1088/1755-1315/169/1/012076.
Koeva, M., Muneza, M., Gevaert, C., Gerke, M., Nex, F., 2016. Survey Review Using UAVs for map creation and updating. A case study in Rwanda Using UAVs for map creation and updating. A case study in Rwanda. Surv. Rev. 50.
Koska, B., Křemen, T., 2013. The combination of laser scanning and structure from motion technology for creation of accurate exterior and interior orthophotos of st. Nicholas Baroque church. Int. Arch. Photogrammetr. Rem. Sens. Spatial Inf. Sci. XL-5/W1. https://doi.org/10.5194/isprsarchives-xl-5-w1-133-2013.
Leitão, J.P., Moy De Vitry, M., Scheidegger, A., Rieckermann, J., 2016. Assessing the quality of digital elevation models obtained from mini unmanned aerial vehicles for overland flow modelling in urban areas. Hydrol. Earth Syst. Sci. 20 (4). https://doi.org/10.5194/hess-20-1637-2016.
Lim, P.C., Rhee, S., Seo, J., Kim, J.I., Chi, J., Lee, S.B., Kim, T., 2021. An optimal image–selection algorithm for large-scale stereoscopic mapping of uav images. Rem. Sens. 13 (11). https://doi.org/10.3390/rs13112118.
Liu, Y., Zheng, X., Ai, G., Zhang, Y., Zuo, Y., 2018. Generating a high-precision true digital orthophoto map based on UAV images. Can. Hist. Rev. 7 (9). https://doi.org/10.3390/ijgi7090333.
Lohani, B., Mason, D.C., 2001. Application of airborne scanning laser altimetry to the study of tidal channel geomorphology. ISPRS J. Photogrammetry Remote Sens. 56 (2). https://doi.org/10.1016/S0924-2716(01)00041-7.
Lowe, D.G., 2004. Distinctive image features from scale-invariant keypoints. Int. J. Comput. Vis. 60 (Issue 2).
Lubansky, A.S., 2011. Rheology and its applications in biotechnology. In: Comprehensive Biotechnology, second ed., vol. 5. https://doi.org/10.1016/B978-0-08-088504-9.00528-6.
Lucieer, A., Jong, S. M. de, Turner, D., 2014. Mapping landslide displacements using Structure from Motion (SfM) and image correlation of multi-temporal UAV photography. Prog. Phys. Geogr. 38 (1). https://doi.org/10.1177/0309133313515293.
Martínez-Espejo Zaragoza, I., Caroti, G., Piemonte, A., Riedel, B., Tengen, D., Niemeier, W., 2017. Structure from motion (SfM) processing of UAV images and combination with terrestrial laser scanning, applied for a 3D-documentation in a hazardous situation. Geomatics, Nat. Hazards Risk 8 (Issue 2). https://doi.org/10.1080/19475705.2017.1345796.
Micheletti, N., Chandler, J.H., Lane, S.N., 2015. Investigating the geomorphological potential of freely available and accessible structure-from-motion photogrammetry using a smartphone. Earth Surf. Process. Landforms 40 (4). https://doi.org/10.1002/esp.3648.
Morgan, J.A., Brogan, D.J., 2016. How to VisualSFM. https://doi.org/10.1109/TPAMI.2009.161.
Ostwald, A.M., Hurtado, J.M., 2017. 3D models from structure-from-motion photogrammetry using mars science laboratory images: methods and implications. Lunar Planet. Sci. XLVIII, 1964.
PIX4D, 2017. PIX4D Documentation - Using GCPs. https://support.pix4d.com/hc/en-us/articles/202558699-Using-GCPs#gsctab=0%202012-2017.
Qin, R., 2014. An object-based hierarchical method for change detection using unmanned aerial vehicle images. Rem. Sens. 6 (9). https://doi.org/10.3390/rs6097911.
Rabiu, L., Waziri, D.A., 2014. Digital orthophoto generation with aerial photographs. Acad. J. Interdiscip. Stud. https://doi.org/10.5901/ajis.2014.v3n7p133.
Raoult, V., Reid-Anderson, S., Ferri, A., Williamson, J., 2017. How reliable is structure from motion (SfM) over time and between observers? A case study using coral reef bommies. Rem. Sens. 9 (7). https://doi.org/10.3390/rs9070740.
Sarp, G., Erener, A., Duzgun, S., Sahin, K., 2014. An approach for detection of buildings and changes in buildings using orthophotos and point clouds: a case study of van erciş earthquake. Eur. J. Rem. Sens. 47 (1). https://doi.org/10.5721/EuJRS20144735.
Shervais, K., 2016. Structure from Motion (SfM) Photogrammetry Field Methods Manual for Students. https://d32ogoqmya1dw8.cloudfront.net/files/getsi/teaching_materials/high-rez-topo/sfm_field_methods_manual.v2.pdf.
Smith, M.W., Vericat, D., 2015. From experimental plots to experimental landscapes: topography, erosion and deposition in sub-humid badlands from Structure-from-Motion photogrammetry. Earth Surf. Process. Landforms 40 (12). https://doi.org/10.1002/esp.3747.
Smith, M.W., Carrivick, J.L., Quincey, D.J., 2016. Structure from motion photogrammetry in physical geography. Prog. Phys. Geogr. 40 (2). https://doi.org/10.1177/0309133315615805.
Tarolli, P., 2014. High-resolution topography for understanding Earth surface processes: opportunities and challenges. Geomorphology 216. https://doi.org/10.1016/j.geomorph.2014.03.008.
Torres-Sánchez, J., López-Granados, F., Borra-Serrano, I., Manuel Peña, J., 2018. Assessing UAV-collected image overlap influence on computation time and digital surface model accuracy in olive orchards. Precis. Agric. 19 (1). https://doi.org/10.1007/s11119-017-9502-0.
Vautherin, J., Rutishauser, S., Schneider-Zapp, K., Choi, H.F., Chovancova, V., Glass, A., Strecha, C., 2016. Photogrammetric accuracy and modeling of rolling shutter cameras. ISPRS Ann. Photogrammetr. Rem. Sens. Spatial Inf. Sci. III–3. https://doi.org/10.5194/isprsannals-iii-3-139-2016.
Westoby, M.J., Brasington, J., Glasser, N.F., Hambrey, M.J., Reynolds, J.M., 2012. "Structure-from-Motion" photogrammetry: a low-cost, effective tool for geoscience applications. Geomorphology 179. https://doi.org/10.1016/j.geomorph.2012.08.021.
World Bank, 2021. Nigeria | Data. https://data.worldbank.org/country/nigeria?view=chart.
Wrózyński, R., Pyszny, K., Sojka, M., Przybyła, C., Murat-Błazejewska, S., 2017. Ground volume assessment using "Structure from Motion" photogrammetry with a smartphone and a compact camera. Open Geosci. 9 (1). https://doi.org/10.1515/geo-2017-0023.
Yao, H., Qin, R., Chen, X., 2019. Unmanned aerial vehicle for remote sensing applications - a review. Rem. Sens. 11 (Issue 12). https://doi.org/10.3390/rs11121443.